THE JOURNAL OF BIOLOGICAL CHEMISTRY VOL. 291, NO. 4, pp. 1676–1691, January 22, 2016

The Structure of a Type 3 Secretion System (T3SS) Ruler Protein Suggests a Molecular Mechanism for Needle Length Sensing*

Received for publication, August 18, 2015, and in revised form, October 29, 2015 Published, JBC Papers in Press, November 20, 2015, DOI 10.1074/jbc.M115.684423

Julien R. C. Bergeron[‡§1], Lucia Fernández[¶2], Gregory A. Wasney[‡], Marija Vuckovic[‡], Fany Reffuveille[¶3], Robert E. W. Hancock[§¶4], and Natalie C. J. Strynadka[‡§5]

From the [‡]Department of Biochemistry and Molecular Biology, the [§]Centre for Blood Research, and the [¶]Centre for Microbial Diseases and Immunity Research, Department of Microbiology and Immunology, University of British Columbia, Vancouver, British Columbia V6T 1Z3, Canada

The type 3 secretion system (T3SS) and the bacterial flagellum are related pathogenicity-associated appendages found at the surface of many disease-causing bacteria. These appendages consist of long tubular structures that protrude away from the bacterial surface to interact with the host cell and/or promote motility. A proposed "ruler" protein tightly regulates the length of both the T3SS and the flagellum, but the molecular basis for this length control has remained poorly characterized and controversial. Using the *Pseudomonas aeruginosa* T3SS as a model system, we report the first structure of a T3SS ruler protein, revealing a "ball-and-chain" architecture, with a globular C-terminal domain (the ball) preceded by a long intrinsically disordered N-terminal polypeptide chain. The dimensions and stability of the globular domain do not support its potential passage through the inner lumen of the T3SS needle. We further demonstrate that a conserved motif at the N terminus of the ruler protein interacts with the T3SS autoprotease in the cytosolic side. Collectively, these data suggest a potential mechanism for needle length sensing by ruler proteins, whereby upon T3SS needle assembly, the ruler protein's N-terminal end is anchored on the cytosolic side, with the globular domain located on the extracellular end of the growing needle. Sequence analysis of T3SS and flagellar ruler proteins shows that this mechanism is probably conserved across systems.

Pathogenic bacteria interact with the cells from infected hosts through a number of multiprotein appendages on their surface, including flagella, fimbriae, pili, and secretion apparatus (1–3). Among these, the bacterial flagellum and the type III secretion system (T3SS)[6] are evolutionarily related (4) and are similar morphologically. Both complexes consist of a basal body portion embedded in and spanning the membrane(s) of the species that encode them, a cytoplasmic export apparatus (also responsible for rotation in the case of the flagellum), and the needle (T3SS) or hook/filament (flagellum) protruding away from the bacterium (5, 6). Both the T3SS and the flagellum possess a number of homologous components, particularly for the export apparatus.

The assembly of the T3SS and flagellum follows a similar, tightly regulated pathway (6–8). First the inner membrane components of the export apparatus and basal body assemble and then recruit the outer membrane proteins. This complex is capable of secreting early effectors, namely the needle (T3SS) and hook (flagellum), which assemble on the extracellular side. Upon completion of these structures, a so-called "substrate switching" event causes the arrest of needle/hook elongation and initiates secretion of the intermediate effectors (tip and translocon for the T3SS, filament for the flagellum). In the case of the T3SS, a second substrate-switching event is triggered by the contact with a target cell, leading to the secretion of late effectors.

Several conserved components of the T3SS and the flagellum have been implicated in substrate switching, primarily the so-called ruler protein (FliK, YscP, Spa32, InvJ, and EscP in the flagellum, *Yersinia* T3SS, *Shigella* T3SS, *Salmonella* SPI-1 T3SS, and enteropathogenic *Escherichia coli* T3SS, respectively), the deletion of which leads to the formation of abnormally long needles in the T3SS (9–14) or of polyhook structures in the flagellum (15, 16). Importantly, ruler proteins are

* This work was supported by operating grants from the Canadian Institute of Health Research (to R. E. W. H and to N. C. J. S.) and the Howard Hughes Medical Institute International Scholar Program (to N. C. J. S.). X-ray diffraction data were collected at beamline 08B1-1 at the Canadian Light Source, which is supported by the Natural Sciences and Engineering Research Council of Canada, the National Research Council Canada, the Canadian Institutes of Health Research, the Province of Saskatchewan, Western Economic Diversification Canada, and the University of Saskatchewan. Instrument support was provided by the Canada Foundation for Innovation, the British Columbia Knowledge Development Fund, the University of British Columbia Blusson Fund, and the Michael Smith Foundation for Health Research. The authors declare that they have no conflicts of interest with the contents of this article.

The atomic coordinates and structure factors (codes 5CUK and 5CUL) have been deposited in the Protein Data Bank (http://wwpdb.org/).

[1] A Michael Smith Foundation for Health Research postdoctoral fellow.

[2] Recipient of a postdoctoral fellowship from the Fundacion Alfonso Martin Escudero (Spain). Present address: Instituto de Productos Lacteos de Asturias, Consejo Superior de Investigaciones Cientificas, Villaviciosa 33300, Asturias, Spain.

[3] Present address: Université de Reims Champagne-Ardennes, Reims 51100, France.

[4] Holder of a Canada Research Chair in Health and Genomics.

[5] Holder of a Canada Research Chair Tier 1 in Antibiotic Discovery. To whom correspondence should be addressed: Dept. of Biochemistry and Molecular Biology, University of British Columbia, Life Sciences Centre, 2350 Health Sciences Mall, Vancouver, British Columbia V6T 1Z3, Canada. Tel.: 604-822-7729; Fax: 604-822-5227; E-mail: ncjs@mail.ubc.ca.

[6] The abbreviations used are: T3SS, type III secretion system; HSQC, heteronuclear single quantum correlation; LS, length-sensing; SS, substrate-switching; SUMO, small ubiquitin-like modifier.

secreted in a T3SS-dependent manner, concomitant with secretion of the early effectors (12, 17–19). Another conserved component (FlhB, YscU, Spa40, SpaS, or EscU, respectively), located in the inner membrane, undergoes spontaneous autoproteolysis of a cytoplasmic loop (20), which is essential for substrate switching (15, 21–25).

In 2003, a remarkable study by the group of Cornelis (26) on the *Yersinia enterocolitica* T3SS ruler protein YscP showed a linear correlation between the length of the *yscP* gene and the length of the T3SS needle. From this observation, the authors hypothesized that YscP physically measures the length of the needle by anchoring on the cytoplasmic and extracellular ends of the needle and spanning through its lumen. In addition, co-expression of two YscP mutant proteins of different length *in vivo* led to two distinct T3SS populations with needle length matching either mutant protein. This supported the model that a single ruler protein regulates needle length in each individual T3SS complex (27). However, the precise mechanism of needle length measurement and substrate switching remains highly controversial, with many competing models being proposed (28–31).

Sequence and mutagenesis analyses of YscP indicate that this protein consists of two domains. At the N-terminal span of the sequence, a predicted helical region is responsible for dictating needle length (referred to as the length-sensing (LS) domain, residues 1–402). In the C-terminal region, a predicted globular domain (residues 403–492; described previously as the type III secretion substrate specificity switch (T3S4) domain, which for clarity we will refer to as the substrate-switching (SS) domain), is necessary for the hierarchical switching of substrates during T3SS assembly and subsequent virulence effector secretion (26, 32).

Here, we report the first structure of a T3SS ruler protein, using the human pathogen *Pseudomonas aeruginosa* as a model system, revealing a "ball-and-chain" architecture consisting of an intrinsically disordered LS domain followed by a globular, highly stable SS domain. The conserved LP*X*LG motif is critical in formation of a β-hairpin that lends to the unusual stability of the SS domain. We also observe that the size and stability of the SS domain would not support its possible secretion through the T3SS needle, suggesting that it is located on the extracellular side prior to needle elongation. Finally, we report the crystal structure of the *P. aeruginosa* autoprotease PscU and demonstrate that it binds to a sequence motif at the N-terminal end of PscP, which is highly conserved across T3SS and flagellar variants. Collectively, these data indicate that the ruler protein is anchored to the cytoplasm at its N terminus, whereas the C-terminal SS domain sits on the extracellular side prior to needle assembly, forming an external anchor. Sequence analysis of other T3SS and flagellar ruler proteins suggests that both the SS domain fold and the interaction between the ruler and autoprotease are probably conserved in all systems, indicative of a common mechanism.

Experimental Procedures

Cloning, Protein Expression, and Purification—All constructs for purification were cloned into the pET28a vector (Novagen), with an N-terminal thrombin-cleavable His_{10} tag, using restriction-free cloning (33). For co-purification experiments, the genes coding for PscU(210–348), PscP(1–369), PscP(1–255) and PscP(256–369) were cloned into pET21a, and the genes coding for PscP(20–40) and PscP(350–369) were cloned into pET SUMO. Point mutations were introduced by site-directed mutagenesis.

Plasmids were transformed into BL21(DE3) competent cells, and transformants were grown to mid-log phase at 37 °C. Protein expression was induced with 1 mM isopropyl 1-thio-β-D-galactopyranoside at 20 °C for 14 h. Cells were harvested at 6,000 × *g* for 15 min, pellets were resuspended in 20 ml of lysis buffer (50 mM HEPES, pH 6.8, 150 mM NaCl with an added protease inhibitor mixture (Roche Applied Science)), and cells were lysed by sonication for 10 min. Proteins were purified from the supernatant using nickel-nitrilotriacetic acid beads (Roche Applied Science) and eluted with lysis buffer containing 500 mM imidazole. The His_{10} tag was cleaved using thrombin (Roche Applied Science) at a 1:1,000 dilution, at 4 °C for 14 h. Proteins were further purified by gel filtration, using a Superdex 75 column (GE Healthcare) in lysis buffer.

For NMR experiments, proteins were expressed in M9 minimal medium containing 1 g/liter ^{15}N-labeled NH_4Cl. Purification was performed as above.

NMR Spectra Acquisition and Assignment—Protein samples were concentrated to 0.2–0.5 mM and dialyzed against 50 mM HEPES, pH 6.8, 10% D_2O. All spectra were collected using a 600-MHz Bruker Avance III spectrometer, equipped with a TCI cryoprobe. Spectra were processed using NMRPipe (34) and analyzed with Sparky (35).

Protein Crystallization and X-ray Crystallographic Structure Determination—Initial crystallization trials were performed by sitting drop vapor diffusion using a Phoenix drop setter (Rigaku). Crystals of PscP(256–369) were obtained in a range of conditions, with optimal diffraction obtained in 0.1 M citric acid, 20% PEG 60000, pH 5.0, at 20 °C. Crystals of PscU(220–341) grew in a range of conditions containing 20% PEG 3350, but these showed no diffraction. In addition, small rod-shaped crystals were obtained at 4 °C in 1 M diammonium hydrogen phosphate, 0.1 M sodium acetate, pH 4.5, that diffracted to ~3 Å.

For data collection, crystals were cryoprotected by soaking in the crystallization condition supplemented with 30% glycerol and flash-cooled in liquid nitrogen. Native data sets were collected at beamline CMCF-1 of the Canadian Light Source, at 100 K. For PscP(256–369), an iodide derivative was obtained by soaking in 0.1 M citric acid, 20% PEG 60000, 0.5 M sodium iodide, pH 5.0, for 10 min, and a data set was collected at a home x-ray source.

The structure of PscP(256–369) was solved by SAD using Phenix (36) and phase information from eight iodide atoms. The structure of PscU(220–341) was solved by molecular replacement with Phaser (37), using the structure of YscU (Protein Data Bank entry 2JLI) (38) as a search model. All data sets were processed with Mosfilm (39) and scaled with Scala (40), and all models were built using Coot (41) and refined with REFMAC5 (42) and Phenix (43).

The PscP(256–369) and PscU(220–341) structures were refined to 2.10 and 2.90 Å resolution, respectively (Table 1), and

both have good stereochemistry, with 98.9 and 95.0% (respectively) of residues in the favored region of the Ramachandran plot with no outliers. We note the presence of density in the PscP(256–369) structure that we attributed to two glycerol molecules, which was present in the cryoprotectant and therefore is unlikely to be biologically relevant.

Symmetry-guided Homology Modeling—For the Rosetta helical modeling, we initially applied the procedure described by DiMaio *et al.* (44), based on the PscF-PrgI alignment shown on Fig. 4*A* and using the solid state NMR-derived PrgI structure (Protein Data Bank entry 2LPZ) for both helical symmetry and homology model template. This led to a number of clusters of models, the lowest energy of which resembled the PrgI needle, but other clusters had an unrealistic conformation with a much larger needle where protomers made very few contacts.

To further help with the conformational space search, we added an additional restraint to the modeling protocol to account for the fit to the MxiH EM map (to avoid model bias), at 25 Å resolution (Electron Microscopy Data Bank ID 1416). This approach led to the modeling procedure converging to a single cluster of models (Fig. 4*B*).

P. aeruginosa Mutant Generation and in Vivo Assay—To obtain an in-frame deletion of *pscP*, we used a three-step fusion PCR (45) construct in which *pscP* was replaced by a gentamicin cassette. Briefly, primers were designed to amplify 1-kb-long fragments flanking *pscP* in the *P. aeruginosa* PA14 chromosome as well as to amplify the gentamicin resistance gene from plasmid pPS858. The resulting fragments were fused via two PCRs. The resulting fragment was cloned into the suicide vector pEX18Amp (46), which was transformed into *E. coli* S17–1λpir, from which it was transferred by conjugation into *P. aeruginosa* strain H103 with a *fliC* mutant to generate deletion of *pscP* by allelic exchange. Colonies carrying the gentamicin cassette were selected by growing the cells from the conjugation on plates containing 30 μg/ml gentamicin for 24–48 h. The obtained colonies were then passed twice on plates containing 15 μg/ml gentamicin and 5% (w/v) sucrose to select for double recombinants. The correct deletion of pscP was subsequently confirmed by PCR and sequencing.

For T3SS expression, we transformed the *P. aeruginosa* strain H103 Δ*fliC* or *P. aeruginosa* strain H103 Δ*fliC*/*pscP* with the plasmid pHERD20T containing the *exsA* gene and grew these in LB medium complemented with 5 mM EGTA, 20 mM $MgCl_2$. Bacteria were grown at 37 °C to mid-log phase, and ExsA expression was induced with 0.02% arabinose at 37 °C for 3 h. Cultures were applied on glow-discharged carbon grids and stained using 0.75% uranyl formate. Images were collected on a Technai G2 transmission electron microscope (FEI) operating at 200 kV and equipped with a high speed AMT 2K side mount CCD camera.

Differential Scanning Calorimetry, Peptide Mapping, and Co-purification Assays—Differential scanning calorimetry experiments were carried out using 0.3 mg/ml protein in the specified buffer, with SYPRO Orange (Life Technologies, Inc.) at 5× final concentration. A 25-μl assay volume mixture was transferred into a MicroAmp Fast optical reaction plate (Applied Biosystems), and thermal denaturation was monitored in an Applied Biosystems StepOnePlus RT-PCR system using the ROX filter set (excitation, 488 nm; emission, 620 nm) at a rate of 1 °C/min from 25 to 95 °C with fluorescence measured every 0.5 °C.

For the peptide-mapping assay, peptides were synthesized directly onto a modified cellulose membrane covalently via a polyethylene glycol linker using a MultiPep peptide synthesizer (Intavis), consisting of 15–17-amino acid segments of the PscP protein sequence for a total of 116 peptides. A 16-polyhistidine peptide was also synthesized as a positive control. The membrane containing the immobilized peptides was washed three times with 0.1% Tween 20 in PBS (PBST) and blocked with 5% skim milk powder in PBST for 1 h followed by washing with PBST and PBS. The membrane was then incubated with 0.3 μM $PscU_C$-His in PBS (or only PBS for the control $PscU_C$-negative experiment) for 1 h at 4 °C, followed by extensive washing with PBST. The membrane was again blocked with 10% skim milk powder in PBST for 1 h, followed by extensive washing with PBST. Next, the membrane was incubated with a 1:5,000-diluted HRP-conjugated anti-His antibody (Alpha Diagnostics) in 5% skim milk powder in PBST for 1 h followed by washing with PBST. Finally, the membrane was developed with ECL reagent (PerkinElmer Life Sciences) and exposed to film for 1 min.

For the co-purification experiments, plasmids for the two proteins or mutants were transformed into competent BL21(DE3) cells and grown in 50 ml of LB at 37 °C to mid-log phase. Expression was induced with 1 mM isopropyl 1-thio-β-D-galactopyranoside, and proteins were expressed at 37 °C for 4 h. Cells were harvested at 6,000 rpm for 15 min, and pellets were resuspended in 1 ml of lysis buffer and sonicated at 40% amplitude for 1 min. Debris was pelleted at 14,000 rpm for 30 min, and the supernatant was incubated with 100 μl of equilibrated nickel-nitrilotriacetic acid beads at 4 °C for 1 h. Beads were pelleted at 14,000 rpm for 15 min, the supernatant was discarded, and the beads were washed twice with 1 ml of lysis buffer and then with 1 ml of lysis buffer containing 75 mM isopropyl 1-thio-β-D-galactopyranoside. Proteins were eluted with 100 μl of lysis buffer complemented with 1 M isopropyl 1-thio-β-D-galactopyranoside. In the case of the co-purification of the PscP domains with His-$PscU_C$, expression of $PscU_C$ was reduced when co-expressed with the SS domain of PscP. To compensate, the various PscP domains were expressed individually, and the cell lysate was added to purified $PscU_C$-His (WT or N263A mutant) prior to the co-purification.

Results

Structure of the P. aeruginosa T3SS Ruler Protein PscP—To characterize the molecular mechanism of needle length control, we attempted to express and purify the *Yersinia* ruler protein YscP, which had been extensively studied. This protein had limited stability and solubility (data not shown), hindering its use for biochemical and structural analysis. However, we were able to purify miligram quantities of the *P. aeruginosa* homologue (47), PscP (20% overall sequence identity to YscP, 40% for the C-terminal SS domain; Fig. 1*A*). PscP possesses an unusual sequence for its N-terminal LS domain, with a Pro-Thr repeat occurring in residues 95–115 (Fig. 1*A*). In addition, this domain was predicted to be intrinsically disordered (not shown), unlike YscP, where it is predicted to be mainly helical (48).

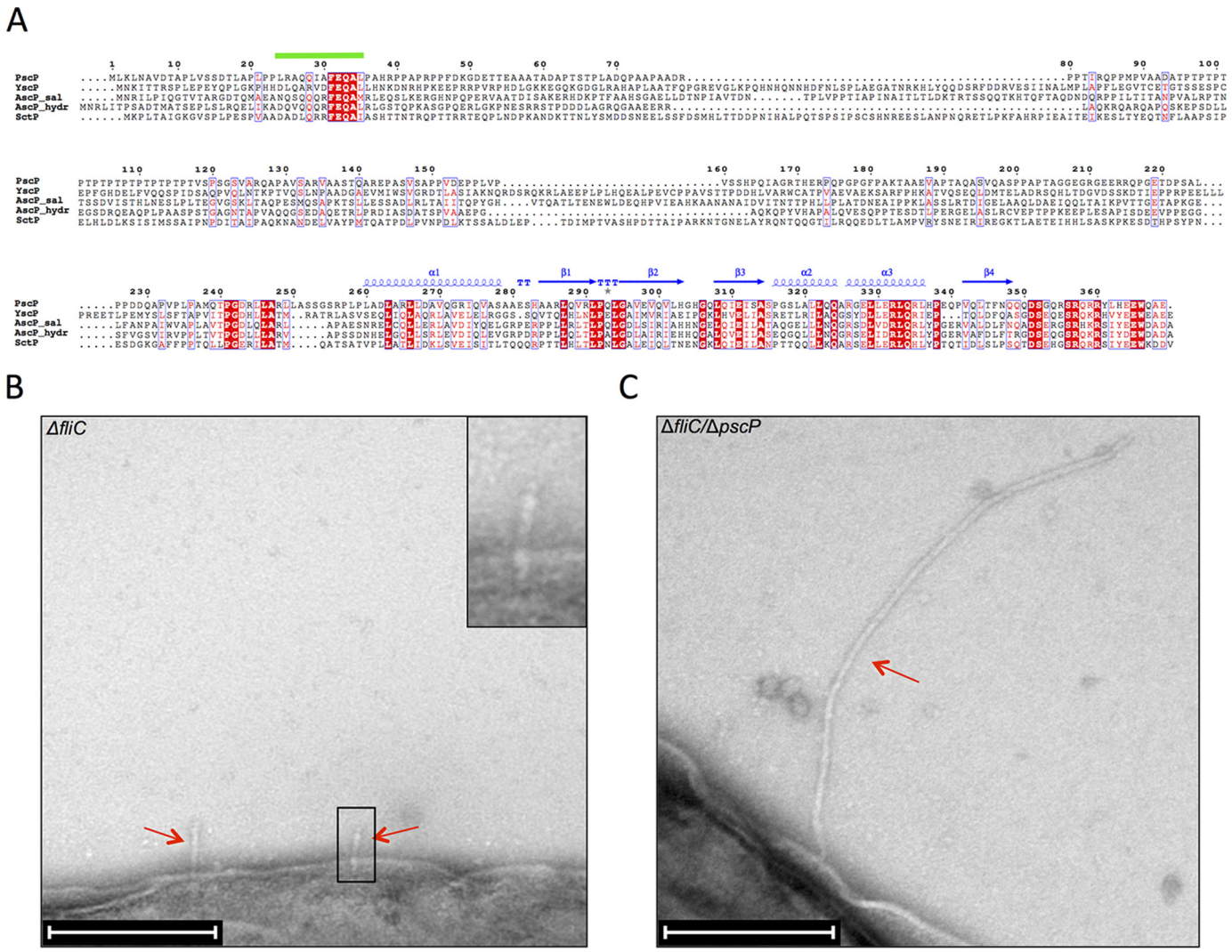

FIGURE 1. **PscP is the *P. aeruginosa* T3SS ruler protein.** *A*, multiple sequence alignment of the SS domain of ruler proteins from the Ysc family (*P. aeruginosa* PscP, *Y. enterocolitica* YscP, *Aeromonas salmonicida* AscP_sal, *Aeromonas hydrophilia* AscP_hydr, *Photorhabdus luminescens* SctP). Secondary structure elements for PscP are shown at the *top*. Conserved residues are *highlighted* in a *solid red box*, and similar residues are shown in *red type*. The *green line* indicates the peptide identified in the peptide-mapping assay (Fig. 6*C*) that interacts with PscU. *B* and *C*, negative stain electron micrographs of *P. aeruginosa* Δ*fliC* (*A*) or Δ*fliC*/Δ*pscP* (*B*) strains overexpressing the T3SS activator ExsA, under T3SS-inducing conditions. *Scale bar*, 200 nm. T3SSs are showed with a *black arrow*. In the Δ*fliC* strain, T3SS needles are observed, with a constant length of ~50 nm. In the Δ*fliC*/Δ*pscP*, needles can reach lengths longer than 1 μm.

PscP can functionally complement a *yscP* deletion strain of *Y. enterocolitica* (32) for needle length control and substrate switching activity *in vivo*, but its role as a ruler protein had not been formally demonstrated in *P. aeruginosa*. To verify this, we deleted the *pscP* gene in a *fliC* deletion strain of *P. aeruginosa* PAO1. When overexpressing the T3SS transcription activator ExsA under T3SS-inducing conditions, we observed, by electron microscopy, T3SS needles of ~50 nm in length at the surface of *P. aeruginosa* bacteria (Fig. 1*B*). In the *pscP* knock-out strain, those T3SS needles were elongated by up to 1 μm (Fig. 1*C*), confirming that PscP is the ruler protein in the *P. aeruginosa* T3SS.

We next used NMR spectroscopy to structurally characterize PscP. As shown in Fig. 2*A*, the ^{15}N HSQC spectrum of full-length PscP (PscP(1–369)) yielded numerous poorly dispersed, sharp peaks between 7.5 and 8.5 ppm on the proton dimension, demonstrating the presence of an extensive intrinsically disordered polypeptide chain. In addition, well dispersed, broader peaks were also observed, indicative of a stably folded protein domain. We postulated that these correspond to the LS and SS domains of the ruler, respectively. Although this could be verified directly by assigning the NMR spectrum of full-length PscP, such a task would be challenging, given the size of the protein and the extensive overlap of its amide signals. Thus, to support our postulate, we cloned and purified the isolated SS domain of PscP (PscP(254–369)). The ^{15}N HSQC spectrum of this construct showed well dispersed peaks that overlapped closely with the subset of dispersed peaks in the spectrum of PscP FL (Fig. 2*A*). This confirmed that, as a purified protein *in vitro*, PscP possesses a ball-and-chain architecture, with a predominantly intrinsically disordered N-terminal LS domain that does not interact significantly with the globular SS domain.

We also obtained crystals of the PscP SS domain and determined its structure to 2.1 Å resolution, by SAD phasing from iodide atoms incorporated using standard labeling procedures (see "Experimental Procedures" and Table 1). The SS domain is

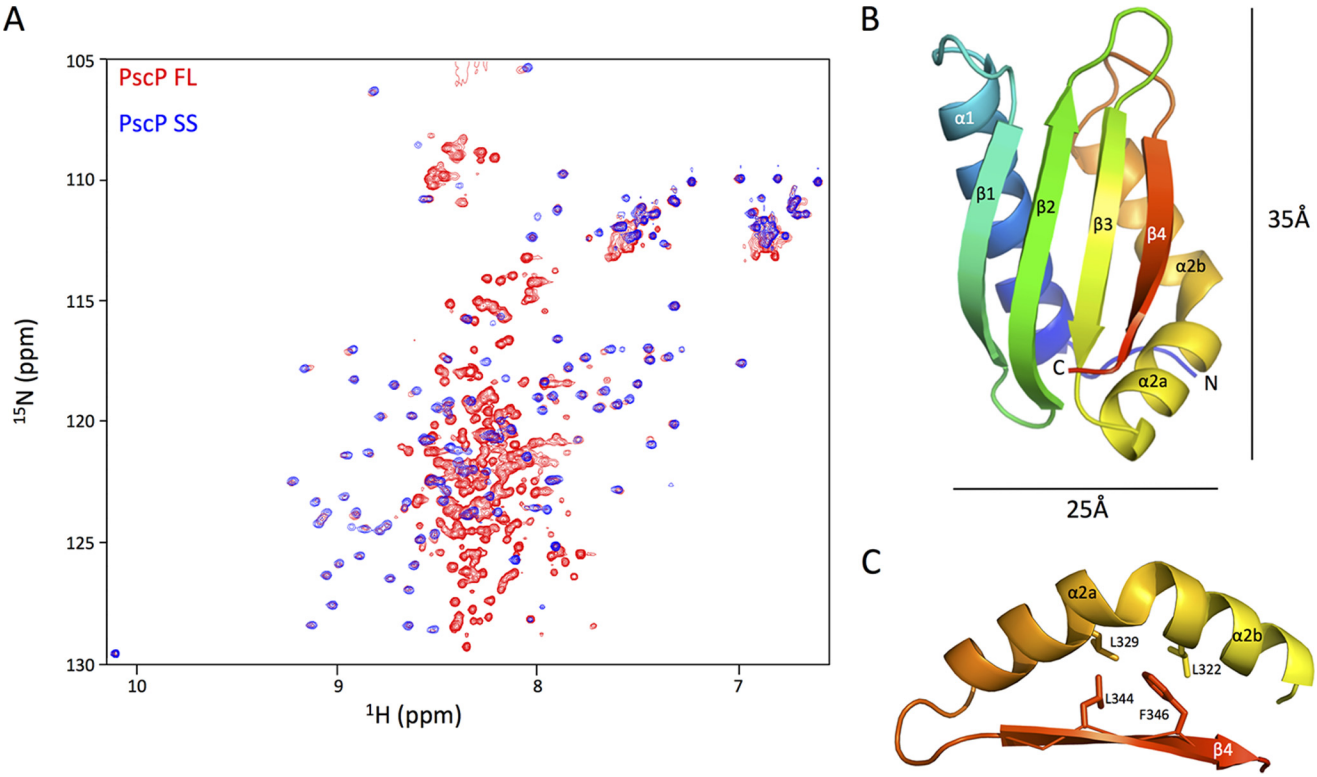

FIGURE 2. **Structure of the *P. aeruginosa* ruler protein PscP.** *A*, the ^{15}N HSQC spectrum of full-length (*FL*) PscP is shown in *red*, and that of the SS domain is overlaid in *blue*. Poorly dispersed, sharp peaks in the center of the FL spectrum indicate intrinsically disordered regions, whereas well dispersed peaks correspond to a globular region. The well dispersed peaks overlay well with the spectrum of the SS domain, confirming that it is globular, whereas the LS domain is disordered. *B*, crystal structure of the SS domain, in a schematic representation. Secondary structure elements and the overall dimensions are indicated. *Rainbow coloring* indicates N to C terminus. *C*, schematic representation of helix α2 and strand β4 of the PscP SS domain. The side chains from bulky residues responsible for the helix break at Ala-325 (ϕ and ψ angles of −105.24 and 14.35°) are shown as *sticks*.

observed to form an elongated shape of ~25 × 22 × 35 Å (Fig. 2*B*), with an overall fold consisting of a four-stranded β-sheet and two α-helices. Helix 2 (residues 317–336) is broken approximately midway (at residue Ala-325), allowing it to more intimately wrap around the hydrophobic core of the SS domain (Fig. 2*B*). The break in helix 2 is stabilized by the presence and packing of four bulky hydrophobic residues in the center of helix 2 and strand 4 (Leu-322, Leu-329, Leu-344, and Phe-346) (Fig. 2*C*). These residues are all conserved, although the interacting phenylalanine and leucine can be swapped in strand 4 in some homologues (Fig. 1*A*). We also note that there is no density observed for residues 350–369 of the crystallized protein, presumably due to the disorder of this region.

The LPXLG Motif Is a Stabilizing β-Turn—One notable element of the ruler SS domain is the conserved LP*X*LG motif (residues 291–295 in PscP; Fig. 1*A*). Previous studies have shown that mutations in this motif lead to an intermediate phenotype, with reduced (but not fully abrogated) substrate switching and needle length control (32). In the PscP crystal structure, we observed that the LP*X*LG motif forms a type II′ β-turn that caps one end of the structure, with the side chains of the two leucine residues (Leu-291 and Leu-294) buried in the hydrophobic core (Fig. 3*A*). Based on this observation, we postulated that the role of this β-turn is to stabilize the fold of the domain.

To verify this, we used differential scanning fluorimetry to quantify the thermal unfolding of PscP in various conditions. Remarkably, as shown in Fig. 3*B*, PscP is a highly stable protein, and no unfolding was observed at temperatures >80 °C under physiological conditions. In the least favorable condition tested (neutral pH, no salt), the midpoint unfolding temperature (T_m) was ~82 °C, with the protein notably stabilized by both lower pH and high salt concentrations. Similarly, subdenaturing concentration of urea stabilized the protein, with a T_m of 87 °C in 2 M urea (Fig. 3*C*).

We next engineered a number of mutations in the LP*X*LG motif of the PscP SS domain and measured their temperature of unfolding. As shown in Fig. 3*C*, mutating either Leu-291 or Leu-294 to alanine significantly decreased its T_m, to 41 and 50 °C, respectively. Furthermore, unlike the wild type protein, urea destabilized both the L291A and L294A mutants, as indicated by decreasing T_m in urea titration. In contrast, mutating the conserved Leu-287, which is exposed on the surface (Fig. 3*A*), marginally increased the T_m to 87 °C. We note that the double LP*X*LG motif mutant L291A/L294A, as well as a mutation of the conserved Leu-322 (buried further in the hydrophobic core; see Fig. 3*A*) to alanine led to proteins being expressed in inclusion bodies (not shown), suggesting that these mutations destabilize the protein to the point that it is no longer soluble.

The PscP SS Domain Cannot Pass through the Needle—It is well established that effector proteins that are transported through the needle are unfolded. Indeed, fusion of small globular domains, such as ubiquitin or GFP, to effector proteins

TABLE 1
Data collection and refinement statistics
Values in parentheses are for the highest resolution shell. r.m.s., root mean square.

	PscP		
	Iodide derivative	Native	PscU (native)
Data collection			
Wavelength (Å)	1.54	0.97949	0.97949
Resolution range (Å)	51.45–2.21 (2.33–2.21)	50.92–2.1 (2.174–2.1)	42.61–2.90 (3.00–2.90)
Space group	C2	C2	P 6_4
Unit cell	104.70, 44.04, 25.74 Å; 90, 100.61, 90°	103.14, 42.48, 25.86 Å; 90, 99.07, 90°	68.59, 68.59, 61.21 Å; 90, 90, 120°
Total reflections	41,303 (5,426)	21,327 (3,172)	7,353 (726)
Unique reflections	5,580 (745)	6,182 (891)	3,694 (365)
Multiplicity	7.4 (7.3)	3.4 (3.6)	2.0 (2.0)
Completeness (%)	95.6 (84.9)	94.6 (93.4)	99.8 (99.7)
Mean $I/\sigma(I)$	16.6 (5.5)	7.2 (2.0)	7.6 (2.0)
R-merge	0.079 (0.349)	0.083 (0.576)	0.087 (0.398)
Refinement			
R-work		0.191	0.196
R-free		0.227	0.226
No. of atoms		774	867
Macromolecules		729	860
Ligands		12	0
Water		33	7
Protein residues		94	107
r.m.s. bonds (Å)		0.012	0.012
r.m.s. angles (degrees)		1.695	1.116
Ramachandran favored (%)		98.9	95
Ramachandran outliers (%)		0	0
Clashscore		14.54	6.26
Average *B*-factor		47.1	54.3
Macromolecules		46.8	54.5
Ligands		60.6	
Solvent		48.2	37.4

abrogates their secretion (49–51) and can cause effectors to be trapped in the needle complex (52, 53). In particular, it has been shown that a YscP-GST fusion blocks effector secretion and needle formation in *Yersinia* (54). Because ruler proteins are secreted early in the T3SS assembly pathway (12, 18), we questioned whether the SS domain of PscP could traverse through the needle. EM analysis of the *P. aeruginosa* (Fig. 1*B*) and the closely related *Y. enterocolitica* T3SS needle (26) confirmed that they are of similar dimension to the *Salmonella* SPI-1 and *Shigella* needle, for which an atomic model based on solid state NMR-derived restraints has been reported (55–57). Based on this, we utilized homology modeling with helical symmetry in the modeling suite Rosetta (44), to generate a PscF needle model using the atomic model of the *Salmonella* SPI-1 T3SS needle (55) as a template (Fig. 4; see "Results" for details). Structural characterization of the *P. aeruginosa* needle protein PscF in its oligomerized form, using a combination of cryo-EM and solid state NMR experiments, will be required to experimentally verify this model. Notably, the sequence conservation between PscF and the *Shigella* needle protein MxiH is limited (23% identity).

The lumen of the *P. aeruginosa* T3SS needle model has a diameter of ~22 Å, similar to that of the *Salmonella* SPI-1 and *Shigella* needle and is proposed to allow passage of unfolded or partially unfolded polypeptides (*e.g.* a single helix). The lumen is narrower than the dimensions of the PscP SS ruler domain (Figs. 2*B* and 4*E*). In order to allow passage of such a domain, a much larger diameter would be required (probably >30 Å, in order to accommodate the water solvation shell surrounding the protein), indicating that significant structural rearrangement either of the needle or of PscP would be required. Considering the stability of the PscP SS domain reported above (Fig. 2), we believe it unlikely that it would unfold prior to secretion. Similarly, significant enlargement of the needle lumen has not been observed in T3SS complexes with trapped effectors (53) and therefore is unlikely to occur while preserving needle integrity. Based on these observations, we propose that the SS ruler domain is recruited to the periplasm prior to needle assembly. Upon needle growth, the domain is probably pushed away at its distal (extracellular aiming) end, the SS domain effectively forming a mechanical anchor at the top of the growing needle. Mutations of the LP*X*LG motif that destabilize the SS domain (see above) might be causing some of these mutant proteins to unfold, thus explaining the intermediate phenotypes observed for these mutations (32).

Structure of the P. aeruginosa Autoprotease PscU—The inner membrane-spanning T3SS autoprotease has also been implicated in substrate switching, and a direct interaction with the ruler protein has been reported in the flagellum and in the enteropathogenic *E. coli* and *Shigella* T3SS systems (14, 58, 59). We therefore purified the cytoplasmic domain from the *P. aeruginosa* autoprotease PscP. As expected, the purified protein PscU(210–348) (hereafter referred to as $PscU_C$) self-cleaved into two fragments of ~7 and ~11 kDa, $PscU_{CN}$ and $PscU_{CC}$ (Fig. 5*A*). We then engineered a N263A mutation in the conserved NPTH loop, where the cleavage event occurs. This led to an intact $PscU_C$ with a molecular mass of ~18 kDa (Fig. 5*A*), confirming that this mutation prevents the self-cleavage of PscU.

We then obtained crystals of PscUc, but these gave very limited diffraction. However, slightly trimming the construct at both ends (PscU(220–341)) yielded crystals with improved diffraction, to 2.9 Å. The structure of this construct was solved by molecular replacement, using the crystallographic coordinates

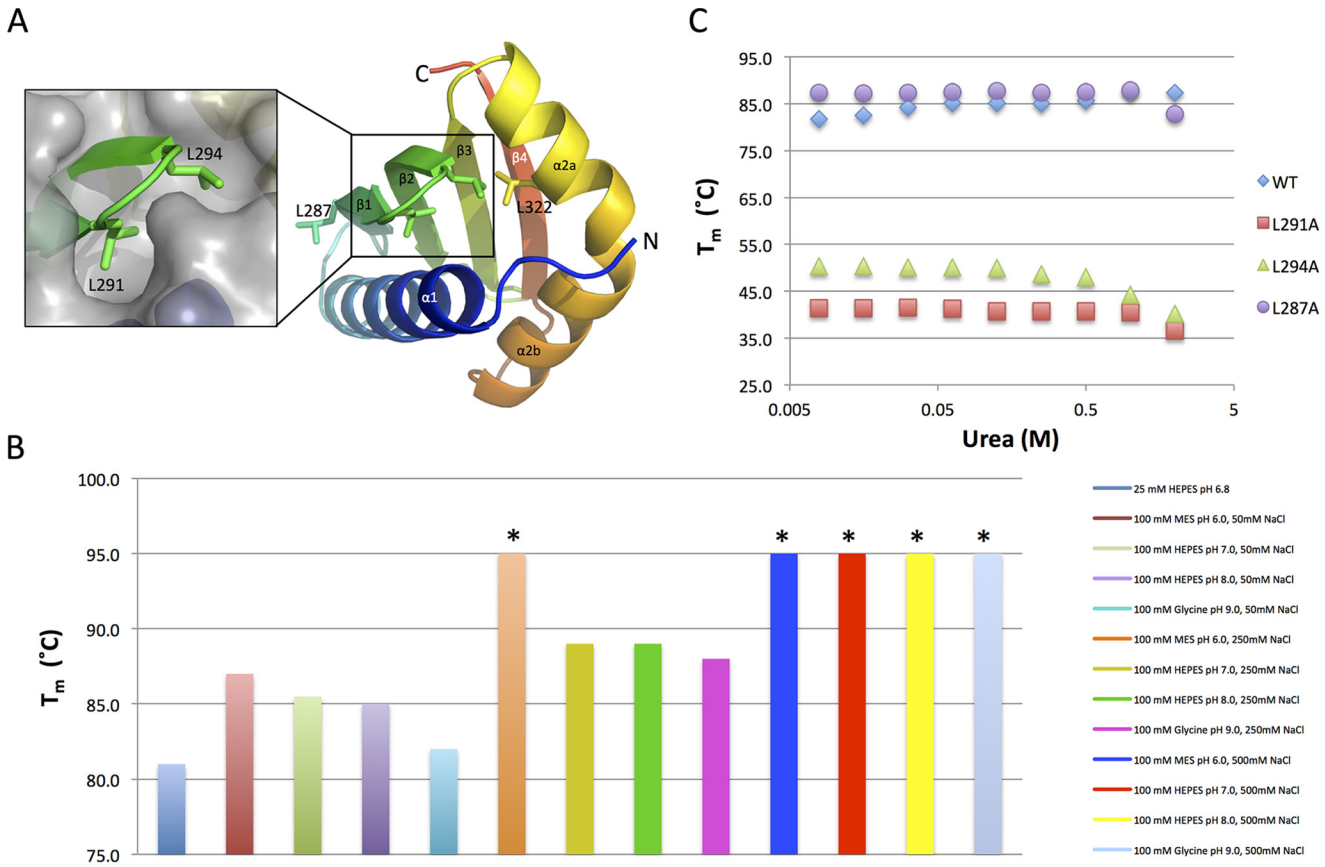

FIGURE 3. **The LPXLG motif provides stabilization of the PscP SS ruler domain.** *A*, the structure of the PscP SS domain is shown in a schematic representation (*rainbow coloring* as in Fig. 2*B*), viewed from the *bottom side*. The side chains for mutated leucine residues are shown as *sticks*. A close-up view of the LPXLG β-turn, with the rest of the protein in surface representation, illustrates the burying of the leucine side chains. *B*, midpoint temperature of unfolding (T_m) for the PscP SS domain in various buffers, with *asterisks* indicating T_m values that are too high to be determined accurately in this assay. *C*, T_m values for the PscP SS domain or mutants, in increasing concentrations of urea. For the WT protein or the L287A mutant, the T_m is >80 °C and is not significantly altered by subdenaturing concentrations of urea. For mutants of the LPXLG loop (L291A and L294A), the T_m is dramatically reduced to ~50 °C, and the protein is further destabilized at subdenaturing concentrations of urea.

of the *Yersinia* autoprotease YscU (Protein Data Bank code 2JLI) (38) as a search model (Table 1). The structure of $PscU_C$, shown in Fig. 5*B*, possesses the canonical autoprotease fold, consisting of a three-stranded β-sheet, surrounded by four α-helices. Residues 230–245, part of the linker region between the transmembrane helices and the globular domain, form a helix (α0) that is largely ordered but does not interact directly with the rest of the protein. As predicted, the bond between Asn-263 and Pro-264 is cleaved in this construct, with the proline amide group pointing away from the generated backbone carboxyl of the catalytic asparagine (Fig. 5*C*).

As illustrated in Fig. 5*D*, whereas the structure of the globular domain of *Pseudomonas* PscU is very similar to that of *Yersinia* YscU (root mean square deviation of 0.68 Å for the backbone atoms of residues 250–338), the orientation of the linker helix α0 differs. The linker region of autoprotease proteins is highly conserved, and a number of mutations in this region were previously shown to affect substrate switching in the enteropathogenic *E. coli* secretion system (20). Interestingly, previous structures of YscU showed that in the wild type protein, the α0 helix was fused to α1, whereas it was separated and interacted with the side of the globular domain in the non-cleavable N263A mutant (Fig. 5*D*), leading to the suggestion that the cleavage of the NPTH loop might lead to rearrangement of the α0 helix. However, in the WT PscU structure reported here, the linker α0 helix is not fused to α1 and is oriented similarly to the YscP N263A mutant. This suggests that the orientation of the α0 helix is not dependent on cleavage of the NPTH loop but that it probably samples a range of conformations in the absence of binding partners and/or membrane insertion.

PscU Autoprotease Interacts with the N Terminus of the PscP Ruler—We next sought to identify the domain of PscP that interacts with PscU. To this end, we co-purified $PscU_C$ with PscP in either the full-length form or with the LS or SS domains only. As shown in Fig. 6*A*, PscP FL and the LS domain co-purified with $PscU_C$ but not the SS domain. We also performed the co-purification assay using the N263A mutant of $PscU_C$ and observed that PscP binding was not affected in this assay (Fig. 6*B*). To more precisely map the region of PscP interacting with $PscU_C$, we performed a peptide array binding assay (60). As shown in Fig. 6*C*, three peptides spanning residues 19–40 of PscP interacted with $PscU_C$ in this assay, as did two peptides spanning residues 350–369. The second set of peptides was probably a false positive, because this region of the protein was present in the PscP SS construct that did not co-elute with $PscU_C$ (Fig. 6*A*). To confirm this, we fused PscP(20–40) or PscP(350–369) at the C terminus of SUMO and observed that $PscU_C$ co-eluted with SUMO-PscP(20–40) but not with

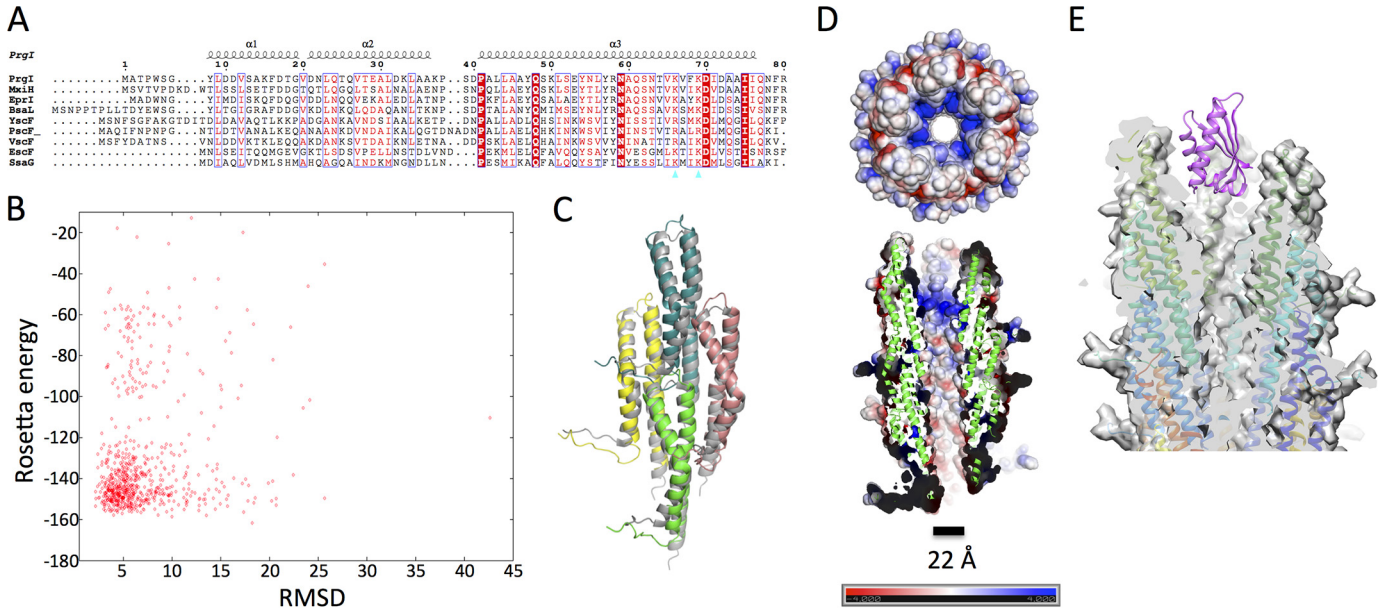

FIGURE 4. **The SS domain of PscP is sterically and thermodynamically incompatible with passage through the T3SS needle.** *A*, multiple sequence alignment of T3SS needle proteins (*Salmonella* SPI-1 PrgI, *Shigella* MxhI, *E. coli* ETT2 EprI, *Burkholderia* T3SS3 BsaL, *Yersinia* YscF, *Pseudomonas* PscF, *Vibrio* VscF, enteropathogenic *E. coli* EscF, *Salmonella* SPI-2 SsaG) with the PrgI secondary structure based on the solid state NMR-derived PrgI structure (Protein Data Bank entry 2LPZ) shown at the *top*. The conserved positively charged residues forming the charged surface at the needle tip are indicated with a *blue triangle*. *Coloring* is as in Fig. 1*C*. *B*, results of the PscF symmetry homology modeling procedure with Rosetta. The energy of each decoy model is plotted *versus* the root mean square deviation to backbone of the lowest energy model. *C*, comparison of the PscF needle model with the PrgI needle structure. Four subunits of the PscF model, corresponding to the repeating unit in the T3SS needle, are shown in *blue*, *yellow*, *orange*, and *green*, overlaid onto similar subunits of the PrgI needle in *gray*. The structures and orientation of PscF subunits are similar to that of PrgI. *D*, the model of the PscF needle is shown in *surface* and *schematic representation*, *colored* by electrostatic charge, viewed from the *top* and *side*. The diameter of the lumen is indicated. *E*, *side view* of the PscF needle model, with the PscP SS structure (*magenta*) shown in the same scale at the *top*. The diameter of the needle lumen is too narrow to accommodate PscP.

SUMO or SUMO-PscP(350–369) (Fig. 6*D*). This demonstrates that residues 20–40 of the PscP ruler protein are sufficient for binding to $PscU_C$.

We also attempted to characterize further the interaction between $PscU_C$ and the SUMO-PscP(20–40) fusion protein using NMR spectroscopy. As shown in Fig. 7*A*, comparison of the ^{15}N HSQC spectra of ^{15}N-labeled SUMO-PscP(20–40) fusion protein in the absence and presence of unlabeled $PscU_C$ revealed that a number of amide $^1H^N$-^{15}N signals disappeared in the bound state. Unfortunately, the SUMO-PscP(20–40) fusion protein was prone to degradation, which prevented the collection of the NMR spectra necessary for HSQC-based assignments. Nonetheless, comparison of the ^{15}N HSQC spectrum of SUMO-PscP(20–40) with that of SUMO (Fig. 7*B*) confirmed that the PscP portion of the fusion protein contributes the peaks affected by binding to $PscU_C$. These peaks also have random coil ^1H chemical shifts, indicating that unbound PscP(20–40) is conformationally disordered. The disappearance of the PscP(20–40) amide signals upon $PscU_C$ binding may result from faster relaxation (line broadening) due to an effective ~18-kDa increase in the mass of SUMO-PscP(20–40). However, the complete absence of new $^1H^N$-^{15}N peaks from the bound complex (and the presence of strong signals from the SUMO residues) suggests additional line broadening of the PscP(20–40) amide signals due to millisecond to microsecond conformational exchange between the free and bound forms of SUMO-PscP(20–40) or within the bound complex.

Remarkably, residues 31–36 of PscP are highly conserved (Fig. 1*A*), with an FEQA(L/I/M) motif found in all of the orthologs of the Ysc family, suggesting that they are important for function. Notably, no sequence conservation could be identified for the rest of the LS domain, except for a PGD*XX*LA motif at residues 241–247 (Fig. 1*A*) at the sequence boundary of the LS and SS domains. We therefore engineered a number of mutations of these residues in the full-length PscP and performed the $PscU_C$ co-purification assay with these. As shown in Fig. 6*E*, all of the F31N, R32R, and F31A/E32A/Q33A mutations (the latter referred to as ΔFEQ) impaired co-elution of PscP with $PscU_C$. A similar result was obtained with the non-cleavable N263A mutant of $PscU_C$ (Fig. 6*F*). We note, however, that the F31N mutant appeared to retain some interaction with $PscU_C$ WT but not with the N263A mutant, perhaps suggesting that the autocleavage affected the interaction. Further biochemical and structural characterization of the PscU-PscP interaction will be required to confirm this observation.

Taken together, these results demonstrate that the conserved FEQA(L/I/M) motif at the N terminus of PscP is necessary and sufficient for binding to $PscU_C$. Importantly, this region has been shown to be necessary for secretion of YscU (61). Based on this, we propose that binding of this motif to PscU serves to recruit PscP to the vicinity of the basal body central cavity, thus acting as a signal sequence.

The Two Ruler Anchors Are Conserved across Systems—Ruler proteins vary widely in size and sequence, with lengths ranging from ~140 amino acids (EscP) to >500 amino acids (YscP) and with no overall significant sequence conservation. Nonetheless, it has been shown that deletion of *Shigella* Spa32 (59) (and, to some extent, *Yersinia* YscP (32)) can be complemented by expression of ruler proteins from other systems, suggesting that the results reported here are not limited to *P. aeruginosa* and

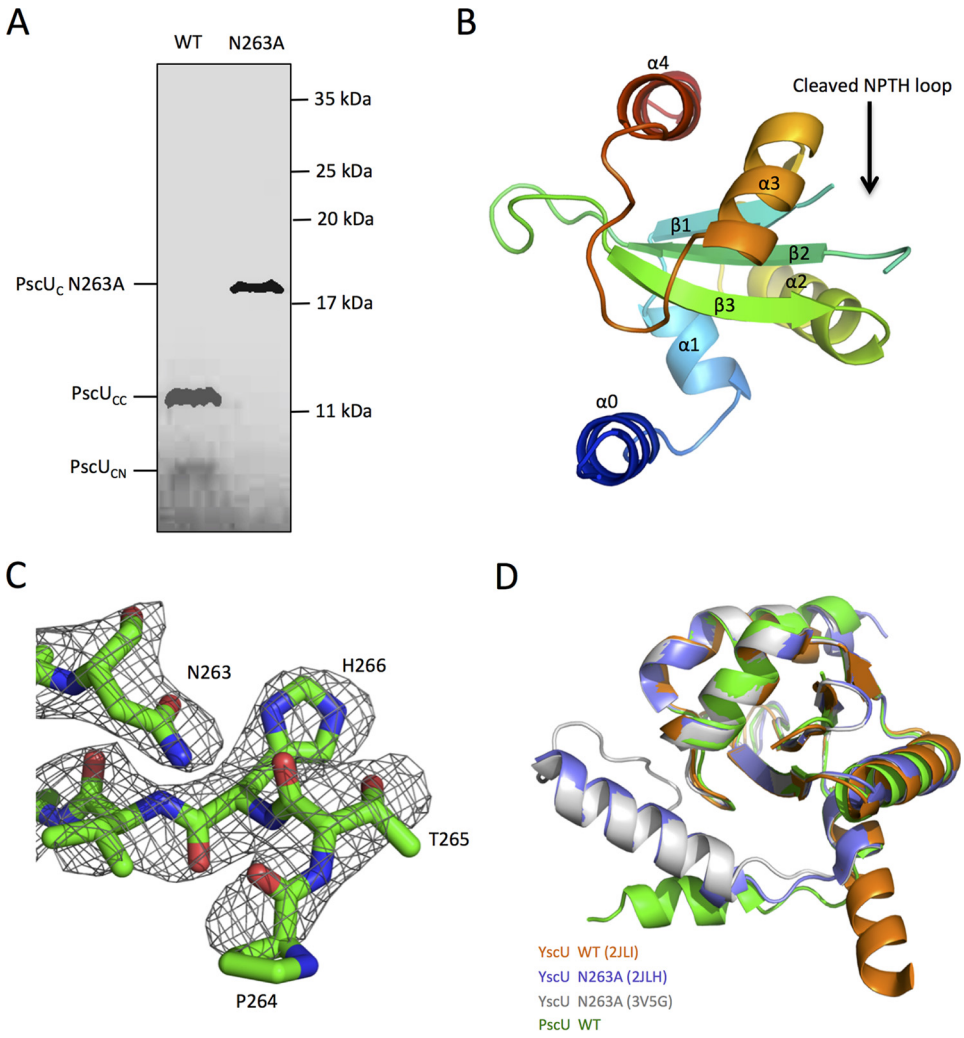

FIGURE 5. **Structure of the *P. aeruginosa* autoprotease PscU.** *A*, Coomassie-stained SDS-polyacrylamide gel of purified PscU$_C$ WT or with a N263A mutation. The WT protein forms two bands of ~7 and 11 kDa (PscU$_{CN}$ and PscU$_{CC}$, respectively), confirming self-cleavage of the NPTH loop. In contrast, the N263A mutant forms a single band at ~18 kDa, indicative that the loop did not cleave. *B*, crystal structure of PscU$_C$, in a *schematic representation*. Secondary structure elements and the location of the NPTH cleavage motif are indicated. *Rainbow coloring* indicates N to C terminus. *C*, *close-up view* of the NPTH motif from the PscU$_C$ crystal structure with the composite OMIT map shown in *gray*. *D*, overlay of the reported structures of YscU$_C$ WT (*orange*), YscU$_C$ N263A (*blue* and *gray*), and PscU$_C$ WT (*green*). The linker helix is oriented differently in the various structures, suggesting that its orientation is probably influenced by crystal packing.

the closely related Ysc family of T3SSs but also apply to other T3SSs as well as to the bacterial flagellum. In support of this, despite their low sequence identity (19% for the SS domain), the previously published solution NMR structure of the flagellum ruler protein FliK (62) shows an architecture similar to that of PscP, with an intrinsically disordered LS domain and a globular SS domain possessing a fold similar to that of PscP (Fig. 8*A*). Secondary structure prediction of other ruler proteins is consistent with a similar SS fold at their C-terminal end (not shown). We also note that the SS domain of FliK possesses an L*X*P*XX*LG motif, between strands β1 and β2, which we propose probably plays a stabilization role similar to that of the LP*X*LG motif of PscP (Fig. 8*B*). Similar motifs are also found in a number of T3SS ruler proteins, such as the *Desulfovibrio* ruler DscP (^{139}LG*XXX*LPG^{146}) and the *Pseudomonas syringae* ruler HrpP (^{129}MP*X*LG^{133}). However, there is not a similar pattern that could be identified in the *Salmonella* SPI-1 (InvJ), SPI-2 (SsaP), enteropathogenic *E. coli* (EscP), or *Shigella* (Spa32) rulers. Nonetheless, our results suggest common secondary structural features for the SS domain of many ruler proteins.

We next gathered ruler proteins from a number of flagellar or T3SS rulers (Table 2) and sought to identify a conserved motif around residues 25–40 of the LS domain, corresponding to the FEQA motif of PscP. As shown in Fig. 8*C* and Table 2, similar sequences were found in most T3SS ruler sequences, including VscP, DscP, EscP, and SsaP. In flagellar ruler proteins, we identified a distinct motif with a different sequence but well conserved across species (residues ^{31}FL*X*LL^{35}). In particular, the location of hydrophobic residues and the conserved phenylalanine indicates that this motif could perform the same function as in the T3SS species. We note that a similar pattern of hydrophobic residues was also found in Spa32 and InvJ, although not including the conserved phenylalanine. Nonetheless, these observations suggest that the binding of the ruler LS domain N terminus to the autoprotease is conserved across systems. Although a direct interaction between FliK and the flagellar

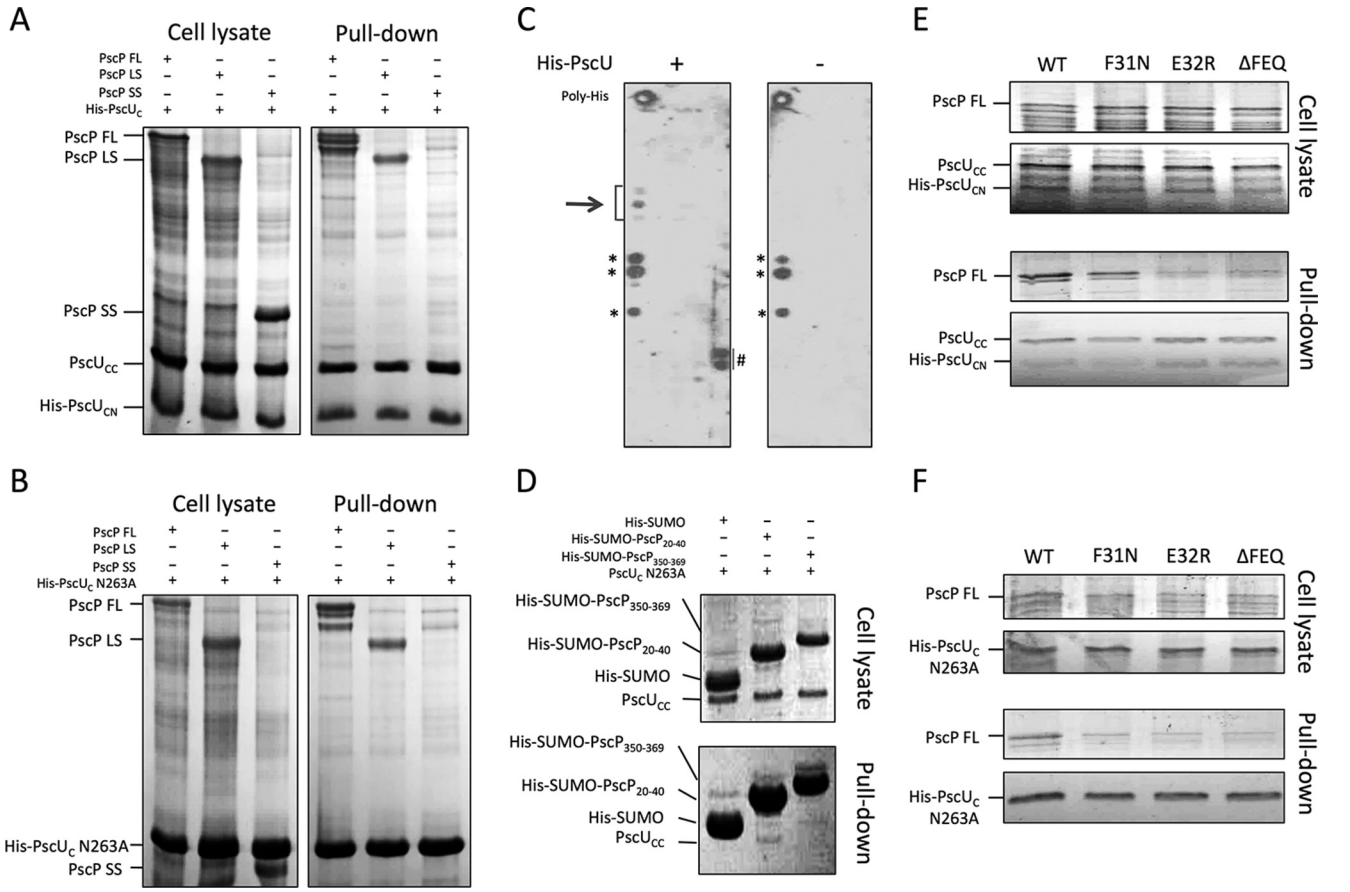

FIGURE 6. **PscU interacts with a conserved FEQA motif in the PscP LS domain.** *A* and *B*, Coomassie-stained SDS-polyacrylamide gel for the co-purification of PscP full length (*FL*), LS domain, or SS domain with PscU$_C$ (*A*) or the N263A mutant (*B*). PscP FL and LS domains co-elute with PscU$_C$ but not the PscP SS domain. *C*, peptide mapping assay for PscU$_C$ binding to PscP. The *top left corner spot* is a His$_9$ peptide control. The *arrow* indicates the FEQA-containing peptides that interact with PscU$_C$. The asterisks indicate peptides that cross-react with the α-His antibody; The number sign indicates false positive peptides that cross-reacted with PscU$_C$ in this assay but not in the pull-down experiments shown in *A* or *D*. *D*, Coomassie-stained SDS-polyacrylamide gel for the co-purification of PscU$_C$ with SUMO fused to PscP peptides. PscU co-purifies with SUMO-PscP(20–40) but not with SUMO or SUMO-PscP(350–369). *E* and *F*, Coomassie-stained SDS-polyacrylamide gel for the co-purification of PscP FL WT or the F31N, E32R, or ΔFEQ mutant with PscU$_C$ (*E*) or the N263A mutant (*F*). The interaction is perturbed by mutations of the FEQA motif.

autoprotease FlhB has been reported (63, 64) and has been shown to occur via the LS domain (58), it remains to be shown that this is mediated by the FL*X*LL motif of FliK.

As noted previously, the LS domains of some ruler orthologues are predicted to be largely helical. We therefore performed a secondary structure prediction for each LS domain and used this to calculate their theoretical length (1.5 Å/residue for helical conformation, 3.5 Å/residue for random coil). In the Ysc family, the theoretical length is between 85 nm (for *Aeromonas* orthologues) and 110 nm (for the *Y. enterocolitica* orthologue) (Table 2). This agrees with the expected length that this domain has to stretch to span the length of the needle (~40 nm for the *Yersinia pestis* and ~55 nm for the *Y. enterocolitica* PscP), both membranes and the periplasmic space (~35 nm), to reach PscU on the cytosolic side (~15 nm), as illustrated in Fig. 9*C*. We have shown here that the LS domain of PscP does not form any secondary structure in isolation, as also suggested by its low sequence complexity that includes a Pro-Thr repeat in residues 95–115. Although, in PscP, the LS domain is significantly shorter than in YscP, their predicted physical lengths are very close due to the formation of α-helices in the latter (Table 2). The role of the Pro-Thr repeat is not known, but it may indicate a sequence repeat expansion that occurred in order to generate longer needles. Indeed, several *P. aeruginosa* strains (such as ATCC, MH27, UCBPP-PA14, and CIG1) exhibit shorter Pro-Thr repeats in the PscP sequence (65), hinting at shorter needles, although this has not been verified experimentally.

Similarly, in the flagellar ruler protein FliK, the theoretical length of the LS domain matches with the length of the flagellum hook (~55 nm in *Salmonella* (15), ~100 nm in *Helicobacter* (66), 120 nm in *Rhodobacter* (67)) added to the span between the outer membrane and the location of the flagellar autoprotease FlhB in the cytosol. We note, however, that for InvJ and Spa32, the theoretical length of the LS domain does not match with that of the T3SS needle (68, 69), taking into account the periplasmic and cytoplasmic space (~70 nm, see Table 2). This could, however, be caused by an excessive estimate of the predicted helical content (56%), because a small decrease to 35% helical would allow the ruler to reach a length of 70 nm. More significantly, we also observe from our analysis that the LS domain of EscP and SsaP is too short to traverse the periplasmic space, even assuming a fully extended conformation. In keeping with this, the systems with shorter needles (enteropathogenic

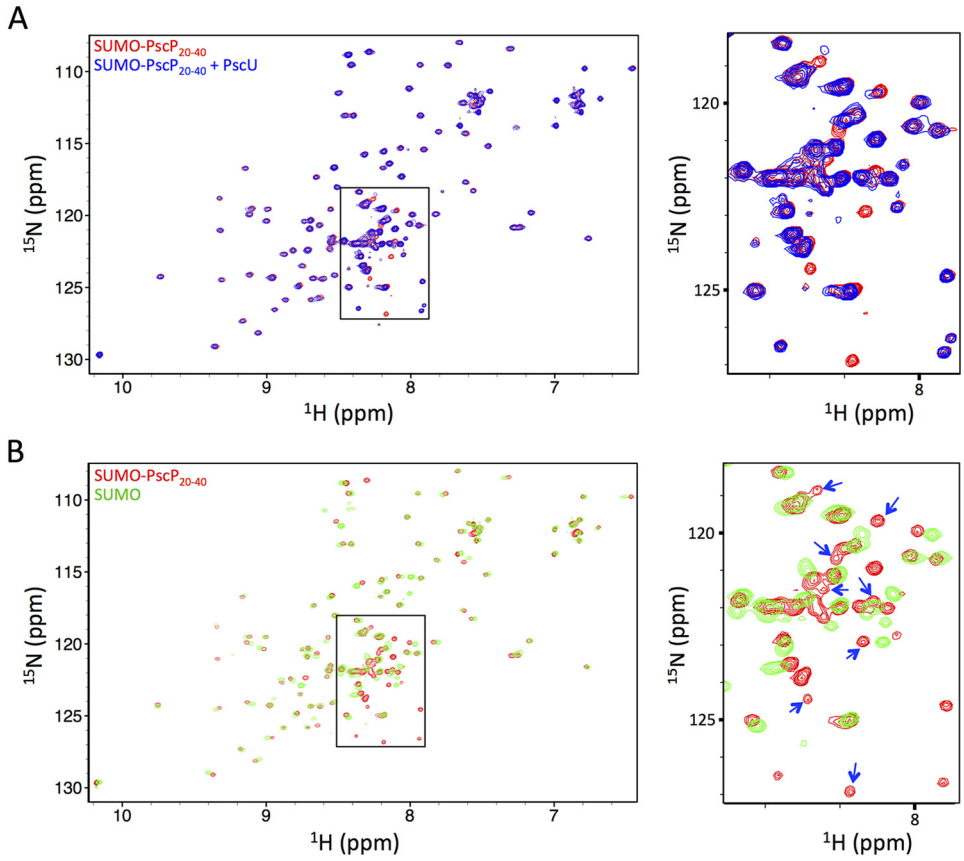

FIGURE 7. **NMR study of the interaction between SUMO-PscP(20–40) and $PscU_C$.** *A*, ^{15}N HSQC spectrum of SUMO-PscP(20–40) (*red*) overlaid onto that of SUMO-PscP(20–40) bound to $PscU_C$ (*blue*). A set of peaks, around the central region of the spectrum, is not present in the bound spectrum, indicative that they are perturbed by $PscU_C$. *B*, ^{15}N HSQC spectrum of SUMO-PscP(20–40) (*red*) overlaid onto that of SUMO (*green*). The peaks not present in the latter spectrum correspond to the PscP peptide. The peaks perturbed by $PscU_C$ in *A* match those yielded by PscP.

E. coli, *Salmonella* SPI-1) also lack the LP*X*LG β-turn (see above). It remains to be established whether this corresponds to mechanistic differences in these systems.

Discussion

In this study, we have demonstrated that PscP, the T3SS ruler from *P. aeruginosa*, has a ball-and-chain architecture with an intrinsically disordered N-terminal LS domain and a globular C-terminal SS domain, the latter of which we report the first structure from a T3SS system ruler protein. We also observe that the size and unusual stability of the SS domain do not seem compatible with its secretion through the T3SS needle. Rather, it may act as a physical anchor at the tip of the growing needle. Finally, we report the crystal structure of the *P. aeruginosa* autoprotease PscU and demonstrate that it interacts with a conserved motif in the LS domain of the PscP ruler. Taken together, these data suggest a model for needle length sensing by ruler proteins, whereby the ruler protein is recruited to the basal body lumen through its interaction with the autoprotease (Fig. 9*A*). We propose that the SS domain is electrostatically pushed away from the growing needle filament (Fig. 9*B*), as supported by the positive charges on the SS interface side and the positive charge at the needle rim on the growing side, formed by the conserved Arg-72 and Arg-75 (Fig. 4*D*). We note that once the ruler protein LS domain is fully extended (Fig. 9*C*), the length of the LS domain matches that of the needle and periplasmic space that it has to traverse. We hypothesize that, at this point, the force on the SS domain necessary for any further growth of the needle leads to the detachment of the N-terminal anchor from the autoprotease (Fig. 9*D*), triggering substrate switching, via a yet unknown mechanism at the cytosolic face of the T3SS apparatus (Fig. 7*E*).

This model for length sensing by the ruler protein marks an important departure from most molecular tape models proposed previously, where the SS domain has systematically been assumed to be located on the cytosolic side. This model, originally proposed by Minamino *et al.* (58) and widely reprised since, arose from the original observation that the SS domain of FliK was responsible for substrate switching. However, the same study demonstrated that it is the LS domain of FliK that interacts with the flagellar autoprotease FlhB, thus supporting the model proposed here.

As noted previously, the mechanism for hook length sensing in the bacterial flagellum is vastly controversial, and a number of alternative mechanisms have been proposed (28–31). Although the similarity in architecture between PscP and FliK (Fig. 8*A*), the conserved self-cleaving of the autoprotease in both systems, and the reported interaction between FliK and the flagellum autoprotease FlhB suggest similar mechanisms, a number of discrepancies have been described. Notably, whereas it has been shown that a single ruler protein controls

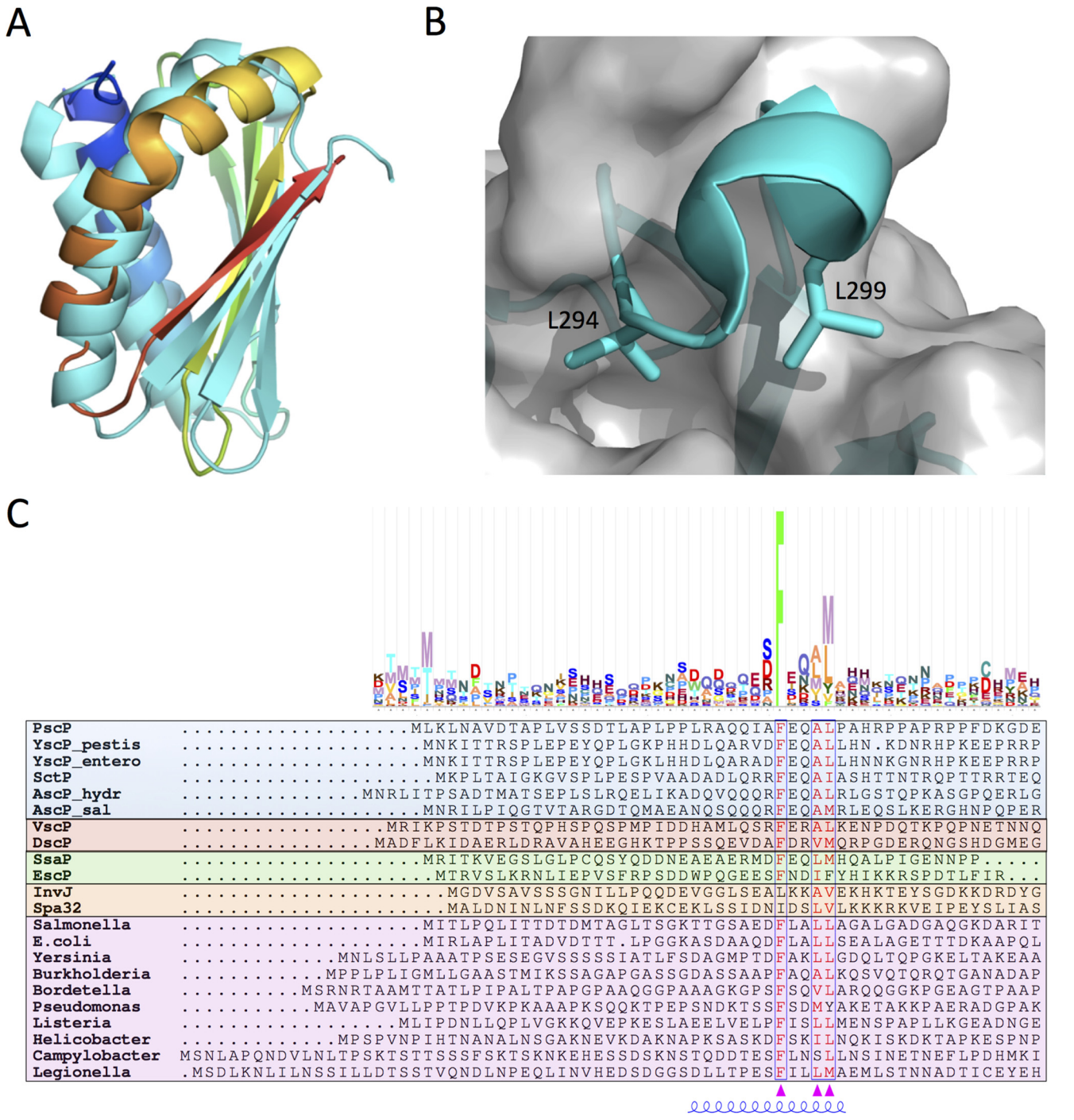

FIGURE 8. **The two ruler anchor motifs are conserved across systems.** *A*, *schematic representation* of the PscP SS domain structure (*rainbow representation*), overlaid onto the structure of FliK (*cyan*), revealing a similar fold. *B*, *close-up view* of the L*X*P*XX*LG loop of FliK, with both leucine residues buried in the hydrophobic core, similar to the LP*X*LG motif of PscP (Fig. 2*A*). *C*, multiple sequence alignment for the first ~50 residues of the LS domains from T3SS and flagellar ruler proteins. The various protein families are *color-coded*, with *cyan* for the Ysc family, *orange* for the Vsd/Dsc family, *green* for the Esc family, *yellow* for the Inv/Mxi family, and *pink* for the flagellum family. The consensus sequence is shown in *WebLogo representation* at the *top*.

needle length in the *Y. enterocolitica* T3SS (27), in the flagellum, several ruler proteins contribute to hook length (70). It is entirely possible that this corresponds to subtle differences between flagellar and T3SS systems, thus explaining the difficulty in reconciling all of the data acquired for both systems. Indeed, the variation in ruler architecture between the various T3SS families (see above) may also correspond to subtle mechanism variation, whereas the general principle of the two anchors is conserved.

In the model reported here, the SS domain acts as a physical anchor at the tip of the nascent needle. This is supported by the size and stability of this domain and probably explains the intermediate phenotype reported for mutants of the LP*X*LG motif in YscP. However, we cannot rule out the possibility that an

TABLE 2
Analysis of the LS domain of ruler proteins from T3SS and flagella

Name	SS domain length (amino acids)	Percentage predicted helical (SS domain)	Predicted length (SS domain)	Anchor motif	Needle length	Reference
		%	*nm*		*nm*	
T3SS rulers						
PscP	259	0 *	90	FEQAL		
YscP (*Y. pestis*)	345	39.1	95	FEQAL	41	Ref. 26
YscP (*Y. enterocolitica*)	408	40.4	110	FEQAL	58	Ref. 26
AscP (*A. hydrophylia*)	250	7.2	84	FEQAL		
AscP (*A. salmonicida*)	326	42.9	86	FEQAM		
SctP	333	31.5	96	FEQAI		
SsaP	46	34.8	13	FEQLM		
EscP	47	25.5	14	FNDIF	23	Ref. 14
InvJ	245	56.4	56	LKKAV	20	Ref. 64
Spa32	197	52.3	48	IDSLV	50	Ref. 65
BsaU	314	25.8	94	LQRAY		
VscP	324	13.3	105	FERAL		
DscP	106	49	27	FDRVM		
HrpP	103	15.5	33	FSQLL		
Flagellum rulers						
Salmonella	267	0*	93	FLALL	55	Ref. 15
E. coli	237	22.8	72	FLALL		
Yersinia	306	63.1	47	FAKLL		
Burkholderia	323	38.7	113	FAQAL		
Bordetella	305	8.5	102	FSQVL		
Pseudomonas	285	30.2	82	FSDMY		
Listeria	218	67.9	47	FISLL		
Helicobacter	385	3.4	132	FSKIL	~100	Ref. 62
Campylobacter	467	68.5	99	FLNSL		
Legionella	285	29.1	83	FILLM		
Treponema	410	55.1	98	FAQSL		
Rhodobacter	575	0	201	FAALL	~120	Ref. 63

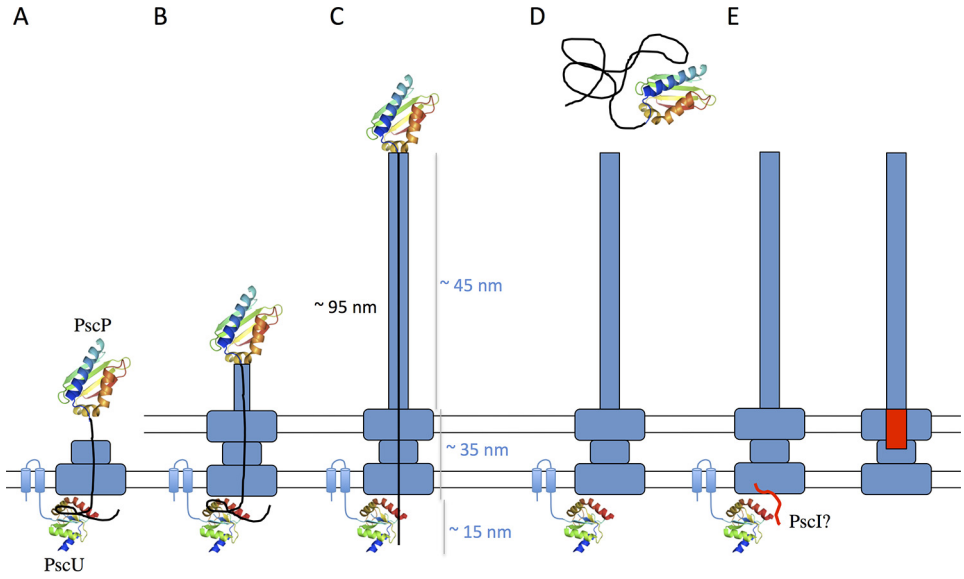

FIGURE 9. **Model of needle length sensing by PscP.** *A*, the N-terminal FEQA motif of PscP interacts with PscU on the cytosolic side, which acts as a secretion signal. *B*, the growing needle pushes the SS domain of PscP, extending the LS domain. *C*, once the LS domain is fully extended, the needle reaches its established length. *D*, ultimately, PscP detaches from PscU and diffuses away in the extracellular space. *E*, in the cytoplasmic space, signals are activated by the PscP displacement, which arrests needle secretion and switches to early effector secretion. We postulate that the rod protein PscI may perform this function.

unidentified protein acts as a ruler chaperone in the cytoplasm, keeping the SS domain unfolded prior to its secretion, or that the needle undergoes major structural rearrangements to allow for the secretion of a folded SS domain. Observation of a ruler protein trapped in a needle complex will be required to further validate the model proposed in Fig. 9.

A second implication of the proposed model is that the SS domain would be located in the periplasmic region of the basal body prior to needle assembly. As noted above, it has been shown that the N terminus of YscP (residues 1–35) is a secretion signal, required for its translocation to the supernatant (61). Because this region overlaps with the PscU-interacting motif that we have identified in PscP, it is likely that this interaction allows for the localization of the PscP SS domain. We note, however, that a second secretion signal was identified in the LS domain of YscP (residues 97–137), and both signals are necessary for efficient secretion of YscP *in vivo* (61). It is therefore likely that additional interactions, possibly with periplasmic elements of the T3SS basal body, are required for localization of the SS domain.

The molecular mechanism of a substrate specificity switch on the cytosolic side remains to be elucidated. The T3SS rod protein (YscI, MxiI, PrgJ, and EscI in the *Yersinia* T3SS, *Shigella* T3SS, *Salmonella* SPI-1 T3SS, and enteropathogenic *E. coli* T3SS, respectively) has been implicated in this process, and direct interaction between the autoprotease and rod has been reported in a number of systems (14, 71–74). However, no obvious rod homologue is found in the flagellum, where four proteins (FlgB, -C, -F, and -G) have been proposed to form a rodlike structure but have not been linked to substrate switching. Finally, we have shown here that the autoprotease interacts with the ruler protein even in a cleavage-deficient mutant (N263A), which does not perform substrate switching *in vivo*. Therefore, the role of the autocleavage event is not explained. It could be envisioned that once the ruler protein dissociates from the autoprotease, the rod protein is recruited in a self-cleavage dependent manner, leading to arrest in needle growth and selection of intermediate effectors (Fig. 3*D*). It is also possible that the autocleavage event weakens the ruler-autoprotease interaction, thus allowing the ruler to dissociate under the pressure exerted by the growing needle. Further biochemical investigation into the interplay between the ruler, rod, and autoprotease will be required to fully understand the substrate selection process in both T3SS and flagellar systems.

Author Contributions—J. R. C. B. performed overexpression, purification, acquisition, and analysis of crystallographic and NMR structural data for all native and mutant proteins as well as the co-purification assays and the PscF filament modeling. J. R. C. B. and G. A. W. contributed to the differential scanning calorimetry and peptide array binding assays, and M. V. contributed to cloning of various constructs. L. F. and F. R. generated the *P. aeruginosa* mutant strains with advice from R. E. W. H., and J. R. B. C. performed the *in vivo* assay and EM analysis. J. R. C. B. and N. C. J. S. analyzed the data and wrote the manuscript with comments from all co-authors.

Acknowledgments—We thank Brianne Burkinshaw for insightful discussions on substrate switching and Matthew Solomonson for suggestions on ruler protein sequence analysis. We acknowledge Lawrence McIntosh and Mark Okon for assistance with NMR data collection.

References

1. Fronzes, R., Remaut, H., and Waksman, G. (2008) Architectures and biogenesis of non-flagellar protein appendages in Gram-negative bacteria. *EMBO J.* **27,** 2271–2280
2. Lebeer, S., Vanderleyden, J., and De Keersmaecker, S. C. (2010) Host interactions of probiotic bacterial surface molecules: comparison with commensals and pathogens. *Nat. Rev. Microbiol.* **8,** 171–184
3. Steadman, D., Lo, A., Waksman, G., and Remaut, H. (2014) Bacterial surface appendages as targets for novel antibacterial therapeutics. *Future Microbiol.* **9,** 887–900
4. Abby, S. S., and Rocha, E. P. (2012) The non-flagellar type III secretion system evolved from the bacterial flagellum and diversified into host-cell adapted systems. *PLoS Genet.* **8,** e1002983
5. Kawamoto, A., Morimoto, Y. V., Miyata, T., Minamino, T., Hughes, K. T., Kato, T., and Namba, K. (2013) Common and distinct structural features of Salmonella injectisome and flagellar basal body. *Sci. Rep.* **3,** 3369
6. Büttner, D. (2012) Protein export according to schedule: architecture, assembly, and regulation of type III secretion systems from plant- and animal-pathogenic bacteria. *Microbiol. Mol. Biol. Rev.* **76,** 262–310
7. Burkinshaw, B. J., and Strynadka, N. C. (2014) Assembly and structure of the T3SS. *Biochim. Biophys. Acta* **1843,** 1649–1663
8. Minamino, T., Imada, K., and Namba, K. (2008) Mechanisms of type III protein export for bacterial flagellar assembly. *Mol. Biosyst.* **4,** 1105–1115
9. Stainier, I., Bleves, S., Josenhans, C., Karmani, L., Kerbourch, C., Lambermont, I., Tötemeyer, S., Boyd, A., and Cornelis, G. R. (2000) YscP, a *Yersinia* protein required for Yop secretion that is surface exposed, and released in low Ca^{2+}. *Mol. Microbiol.* **37,** 1005–1018
10. Edqvist, P. J., Olsson, J., Lavander, M., Sundberg, L., Forsberg, A., Wolf-Watz, H., and Lloyd, S. A. (2003) YscP and YscU regulate substrate specificity of the *Yersinia* type III secretion system. *J. Bacteriol.* **185,** 2259–2266
11. Magdalena, J., Hachani, A., Chamekh, M., Jouihri, N., Gounon, P., Blocker, A., and Allaoui, A. (2002) Spa32 regulates a switch in substrate specificity of the type III secreton of *Shigella flexneri* from needle components to Ipa proteins. *J. Bacteriol.* **184,** 3433–3441
12. Tamano, K., Katayama, E., Toyotome, T., and Sasakawa, C. (2002) Shigella Spa32 is an essential secretory protein for functional type III secretion machinery and uniformity of its needle length. *J. Bacteriol.* **184,** 1244–1252
13. Kubori, T., Sukhan, A., Aizawa, S. I., and Galán, J. E. (2000) Molecular characterization and assembly of the needle complex of the *Salmonella typhimurium* type III protein secretion system. *Proc. Natl. Acad. Sci. U.S.A.* **97,** 10225–10230
14. Monjarás Feria, J., Garcia-Gómez, E., Espinosa, N., Minamino, T., Namba, K., and González-Pedrajo, B. (2012) Role of EscP (Orf16) in injectisome biogenesis and regulation of type III protein secretion in enteropathogenic *Escherichia coli*. *J. Bacteriol.* **194,** 6029–6045
15. Hirano, T., Yamaguchi, S., Oosawa, K., and Aizawa, S. (1994) Roles of FliK and FlhB in determination of flagellar hook length in *Salmonella typhimurium*. *J. Bacteriol.* **176,** 5439–5449
16. Kawagishi, I., Homma, M., Williams, A. W., and Macnab, R. M. (1996) Characterization of the flagellar hook length control protein fliK of Salmonella typhimurium and *Escherichia coli*. *J. Bacteriol.* **178,** 2954–2959
17. Minamino, T., González-Pedrajo, B., Yamaguchi, K., Aizawa, S. I., and Macnab, R. M. (1999) FliK, the protein responsible for flagellar hook length control in *Salmonella*, is exported during hook assembly. *Mol. Microbiol.* **34,** 295–304
18. Payne, P. L., and Straley, S. C. (1999) YscP of *Yersinia pestis* is a secreted component of the Yop secretion system. *J. Bacteriol.* **181,** 2852–2862
19. Rüssmann, H., Kubori, T., Sauer, J., and Galán, J. E. (2002) Molecular and functional analysis of the type III secretion signal of the *Salmonella enterica* InvJ protein. *Mol. Microbiol.* **46,** 769–779
20. Zarivach, R., Deng, W., Vuckovic, M., Felise, H. B., Nguyen, H. V., Miller, S. I., Finlay, B. B., and Strynadka, N. C. (2008) Structural analysis of the essential self-cleaving type III secretion proteins EscU and SpaS. *Nature* **453,** 124–127
21. Minamino, T., and Macnab, R. M. (2000) Domain structure of *Salmonella* FlhB, a flagellar export component responsible for substrate specificity switching. *J. Bacteriol.* **182,** 4906–4914
22. Lavander, M., Sundberg, L., Edqvist, P. J., Lloyd, S. A., Wolf-Watz, H., and Forsberg, A. (2002) Proteolytic cleavage of the FlhB homologue YscU of *Yersinia* pseudotuberculosis is essential for bacterial survival but not for type III secretion. *J. Bacteriol.* **184,** 4500–4509
23. Fraser, G. M., Hirano, T., Ferris, H. U., Devgan, L. L., Kihara, M., and Macnab, R. M. (2003) Substrate specificity of type III flagellar protein export in *Salmonella* is controlled by subdomain interactions in FlhB. *Mol. Microbiol.* **48,** 1043–1057
24. Ferris, H. U., Furukawa, Y., Minamino, T., Kroetz, M. B., Kihara, M., Namba, K., and Macnab, R. M. (2005) FlhB regulates ordered export of flagellar components via autocleavage mechanism. *J. Biol. Chem.* **280,** 41236–41242
25. Deane, J. E., Graham, S. C., Mitchell, E. P., Flot, D., Johnson, S., and Lea, S. M. (2008) Crystal structure of Spa40, the specificity switch for the *Shigella flexneri* type III secretion system. *Mol. Microbiol.* **69,** 267–276
26. Journet, L., Agrain, C., Broz, P., and Cornelis, G. R. (2003) The needle length of bacterial injectisomes is determined by a molecular ruler. *Science* **302,** 1757–1760
27. Wagner, S., Stenta, M., Metzger, L. C., Dal Peraro, M., and Cornelis, G. R.

(2010) Length control of the injectisome needle requires only one molecule of Yop secretion protein P (YscP). *Proc. Natl. Acad. Sci. U.S.A.* **107,** 13860–13865
28. Aizawa, S. (2012) Rebuttal: flagellar hook length is controlled by a secreted molecular ruler. *J. Bacteriol.* **194,** 4797
29. Hughes, K. T. (2012) Flagellar hook length is controlled by a secreted molecular ruler. *J. Bacteriol.* **194,** 4793–4796
30. Aizawa, S. (2012) Mystery of fliK in length control of the flagellar hook. *J. Bacteriol.* **194,** 4798–4800
31. Hughes, K. T. (2012) Rebuttal: mystery of FliK in length control of the flagellar hook. *J. Bacteriol.* **194,** 4801
32. Agrain, C., Callebaut, I., Journet, L., Sorg, I., Paroz, C., Mota, L. J., and Cornelis, G. R. (2005) Characterization of a type III secretion substrate specificity switch (T3S4) domain in YscP from *Yersinia enterocolitica*. *Mol. Microbiol.* **56,** 54–67
33. van den Ent, F., and Löwe, J. (2006) RF cloning: a restriction-free method for inserting target genes into plasmids. *J. Biochem. Biophys. Methods* **67,** 67–74
34. Delaglio, F., Grzesiek, S., Vuister, G. W., Zhu, G., Pfeifer, J., and Bax, A. (1995) NMRPipe: a multidimensional spectral processing system based on UNIX pipes. *J. Biomol. NMR* **6,** 277–293
35. Small, J. (1983) Sparky. *Geriatr. Nurs.* **4,** 166
36. Adams, P. D., Afonine, P. V., Bunkóczi, G., Chen, V. B., Echols, N., Headd, J. J., Hung, L. W., Jain, S., Kapral, G. J., Grosse Kunstleve, R. W., McCoy, A. J., Moriarty, N. W., Oeffner, R. D., Read, R. J., Richardson, D. C., Richardson, J. S., Terwilliger, T. C., and Zwart, P. H. (2011) The Phenix software for automated determination of macromolecular structures. *Methods* **55,** 94–106
37. McCoy, A. J. (2007) Solving structures of protein complexes by molecular replacement with Phaser. *Acta Crystallogr. D Biol. Crystallogr.* **63,** 32–41
38. Lountos, G. T., Austin, B. P., Nallamsetty, S., and Waugh, D. S. (2009) Atomic resolution structure of the cytoplasmic domain of *Yersinia pestis* YscU, a regulatory switch involved in type III secretion. *Protein Sci.* **18,** 467–474
39. Battye, T. G., Kontogiannis, L., Johnson, O., Powell, H. R., and Leslie, A. G. (2011) iMOSFLM: a new graphical interface for diffraction-image processing with MOSFLM. *Acta Crystallogr. D Biol. Crystallogr.* **67,** 271–281
40. Winn, M. D., Ballard, C. C., Cowtan, K. D., Dodson, E. J., Emsley, P., Evans, P. R., Keegan, R. M., Krissinel, E. B., Leslie, A. G., McCoy, A., McNicholas, S. J., Murshudov, G. N., Pannu, N. S., Potterton, E. A., Powell, H. R., Read, R. J., Vagin, A., and Wilson, K. S. (2011) Overview of the CCP4 suite and current developments. *Acta Crystallogr. D Biol. Crystallogr.* **67,** 235–242
41. Emsley, P., Lohkamp, B., Scott, W. G., and Cowtan, K. (2010) Features and development of Coot. *Acta Crystallogr. D Biol. Crystallogr.* **66,** 486–501
42. Murshudov, G. N., Skubák, P., Lebedev, A. A., Pannu, N. S., Steiner, R. A., Nicholls, R. A., Winn, M. D., Long, F., and Vagin, A. A. (2011) REFMAC5 for the refinement of macromolecular crystal structures. *Acta Crystallogr. D Biol. Crystallogr.* **67,** 355–367
43. Afonine, P. V., Grosse-Kunstleve, R. W., Echols, N., Headd, J. J., Moriarty, N. W., Mustyakimov, M., Terwilliger, T. C., Urzhumtsev, A., Zwart, P. H., and Adams, P. D. (2012) Towards automated crystallographic structure refinement with phenix.refine. *Acta Crystallogr. D Biol. Crystallogr.* **68,** 352–367
44. DiMaio, F., Leaver-Fay, A., Bradley, P., Baker, D., and André, I. (2011) Modeling symmetric macromolecular structures in Rosetta3. *PLoS One* **6,** e20450
45. Kuwayama, H., Obara, S., Morio, T., Katoh, M., Urushihara, H., and Tanaka, Y. (2002) PCR-mediated generation of a gene disruption construct without the use of DNA ligase and plasmid vectors. *Nucleic Acids Res.* **30,** E2
46. Hoang, T. T., Karkhoff-Schweizer, R. R., Kutchma, A. J., and Schweizer, H. P. (1998) A broad-host-range Flp-FRT recombination system for site-specific excision of chromosomally-located DNA sequences: application for isolation of unmarked *Pseudomonas aeruginosa* mutants. *Gene* **212,** 77–86
47. Troisfontaines, P., and Cornelis, G. R. (2005) Type III secretion: more systems than you think. *Physiology* **20,** 326–339
48. Wagner, S., Sorg, I., Degiacomi, M., Journet, L., Dal Peraro, M., and Cornelis, G. R. (2009) The helical content of the YscP molecular ruler determines the length of the *Yersinia* injectisome. *Mol. Microbiol.* **71,** 692–701
49. Feldman, M. F., Müller, S., Wüest, E., and Cornelis, G. R. (2002) SycE allows secretion of YopE-DHFR hybrids by the *Yersinia enterocolitica* type III Ysc system. *Mol. Microbiol.* **46,** 1183–1197
50. Lee, V. T., and Schneewind, O. (2002) Yop fusions to tightly folded protein domains and their effects on *Yersinia enterocolitica* type III secretion. *J. Bacteriol.* **184,** 3740–3745
51. Sorg, J. A., Blaylock, B., and Schneewind, O. (2006) Secretion signal recognition by YscN, the *Yersinia* type III secretion ATPase. *Proc. Natl. Acad. Sci. U.S.A.* **103,** 16490–16495
52. Dohlich, K., Zumsteg, A. B., Goosmann, C., and Kolbe, M. (2014) A substrate-fusion protein is trapped inside the type III secretion system channel in *Shigella flexneri*. *PLoS Pathog.* **10,** e1003881
53. Radics, J., Königsmaier, L., and Marlovits, T. C. (2014) Structure of a pathogenic type 3 secretion system in action. *Nat. Struct. Mol. Biol.* **21,** 82–87
54. Riordan, K. E., Sorg, J. A., Berube, B. J., and Schneewind, O. (2008) Impassable YscP substrates and their impact on the *Yersinia enterocolitica* type III secretion pathway. *J. Bacteriol.* **190,** 6204–6216
55. Loquet, A., Sgourakis, N. G., Gupta, R., Giller, K., Riedel, D., Goosmann, C., Griesinger, C., Kolbe, M., Baker, D., Becker, S., and Lange, A. (2012) Atomic model of the type III secretion system needle. *Nature* **486,** 276–279
56. Demers, J. P., Sgourakis, N. G., Gupta, R., Loquet, A., Giller, K., Riedel, D., Laube, B., Kolbe, M., Baker, D., Becker, S., and Lange, A. (2013) The common structural architecture of *Shigella flexneri* and *Salmonella typhimurium* type three secretion needles. *PLoS Pathog.* **9,** e1003245
57. Demers, J. P., Habenstein, B., Loquet, A., Kumar Vasa, S., Giller, K., Becker, S., Baker, D., Lange, A., and Sgourakis, N. G. (2014) High-resolution structure of the Shigella type-III secretion needle by solid-state NMR and cryo-electron microscopy. *Nat. Commun.* **5,** 4976
58. Minamino, T., Saijo-Hamano, Y., Furukawa, Y., González-Pedrajo, B., Macnab, R. M., and Namba, K. (2004) Domain organization and function of *Salmonella* FliK, a flagellar hook-length control protein. *J. Mol. Biol.* **341,** 491–502
59. Botteaux, A., Sani, M., Kayath, C. A., Boekema, E. J., and Allaoui, A. (2008) Spa32 interaction with the inner-membrane Spa40 component of the type III secretion system of *Shigella flexneri* is required for the control of the needle length by a molecular tape measure mechanism. *Mol. Microbiol.* **70,** 1515–1528
60. Nady, N., Min, J., Kareta, M. S., Chédin, F., and Arrowsmith, C. H. (2008) A SPOT on the chromatin landscape? Histone peptide arrays as a tool for epigenetic research. *Trends Biochem. Sci.* **33,** 305–313
61. Agrain, C., Sorg, I., Paroz, C., and Cornelis, G. R. (2005) Secretion of YscP from *Yersinia enterocolitica* is essential to control the length of the injectisome needle but not to change the type III secretion substrate specificity. *Mol. Microbiol.* **57,** 1415–1427
62. Mizuno, S., Amida, H., Kobayashi, N., Aizawa, S., and Tate, S. (2011) The NMR structure of FliK, the trigger for the switch of substrate specificity in the flagellar type III secretion apparatus. *J. Mol. Biol.* **409,** 558–573
63. McMurry, J. L., Minamino, T., Furukawa, Y., Francis, J. W., Hill, S. A., Helms, K. A., and Namba, K. (2015) Weak interactions between *Salmonella enterica* FlhB and other flagellar export apparatus proteins govern type III secretion dynamics. *PLoS One* **10,** e0134884
64. Morris, D. P., Roush, E. D., Thompson, J. W., Moseley, M. A., Murphy, J. W., and McMurry, J. L. (2010) Kinetic characterization of *Salmonella* FliK-FlhB interactions demonstrates complexity of the Type III secretion substrate-specificity switch. *Biochemistry* **49,** 6386–6393
65. Winsor, G. L., Lam, D. K., Fleming, L., Lo, R., Whiteside, M. D., Yu, N. Y., Hancock, R. E., and Brinkman, F. S. (2011) *Pseudomonas* genome database: improved comparative analysis and population genomics capability for *Pseudomonas* genomes. *Nucleic Acids Res.* **39,** D596–D600
66. Ryan, K. A., Karim, N., Worku, M., Penn, C. W., and O'Toole, P. W. (2005) *Helicobacter pylori* flagellar hook-filament transition is controlled by a FliK functional homolog encoded by the gene HP0906. *J. Bacteriol.* **187,** 5742–5750

67. Kobayashi, K., Saitoh, T., Shah, D. S., Ohnishi, K., Goodfellow, I. G., Sockett, R. E., and Aizawa, S. I. (2003) Purification and characterization of the flagellar basal body of *Rhodobacter sphaeroides*. *J. Bacteriol.* **185,** 5295–5300
68. Wee, D. H., and Hughes, K. T. (2015) Molecular ruler determines needle length for the *Salmonella* Spi-1 injectisome. *Proc. Natl. Acad. Sci. U.S.A.* **112,** 4098–4103
69. Cordes, F. S., Komoriya, K., Larquet, E., Yang, S., Egelman, E. H., Blocker, A., and Lea, S. M. (2003) Helical structure of the needle of the type III secretion system of *Shigella flexneri*. *J. Biol. Chem.* **278,** 17103–17107
70. Erhardt, M., Singer, H. M., Wee, D. H., Keener, J. P., and Hughes, K. T. (2011) An infrequent molecular ruler controls flagellar hook length in *Salmonella enterica*. *EMBO J.* **30,** 2948–2961
71. Wood, S. E., Jin, J., and Lloyd, S. A. (2008) YscP and YscU switch the substrate specificity of the *Yersinia* type III secretion system by regulating export of the inner rod protein YscI. *J. Bacteriol.* **190,** 4252–4262
72. Sal-Man, N., Deng, W., and Finlay, B. B. (2012) EscI: a crucial component of the type III secretion system forms the inner rod structure in enteropathogenic *Escherichia coli*. *Biochem. J.* **442,** 119–125
73. Marlovits, T. C., Kubori, T., Lara-Tejero, M., Thomas, D., Unger, V. M., and Galán, J. E. (2006) Assembly of the inner rod determines needle length in the type III secretion injectisome. *Nature* **441,** 637–640
74. Burkinshaw, B. J., Deng, W., Lameignère, E., Wasney, G. A., Zhu, H., Worrall, L. J., Finlay, B. B., and Strynadka, N. C. (2015) Structural analysis of a specialized type III secretion system peptidoglycan-cleaving enzyme. *J. Biol. Chem.* **290,** 10406–10417